Systematic feedback control design for scattered light noise mitigation in Virgo's MultiSAS

Systematic feedback control design for scattered light noise mitigation in Virgo's MultiSAS

Mathyn van Dael*‡, Gert Witvoet*†, Bas Swinkels‡ and Tom Oomen*◇
* *Eindhoven University of Technology, dept. of Mechanical Engineering, Control Systems Technology*
Eindhoven, The Netherlands, email: m.r.v.dael@tue.nl
† TNO, Optomechatronics Department, Delft, The Netherlands
‡ Nikhef, Amsterdam, The Netherlands
◇ Delft Center for Systems and Control, Delft University of Technology, Delft, The Netherlands

***Abstract*—Gravitational Wave (GW) detectors are used to gather knowledge on violent cosmic events like the merger of pairs of black holes. These waves are measured using large-scale interferometers, which detect the undulations in *spacetime* resulting from GWs. Scattered light noise resulting from the horizontal RMS velocity of auxiliary optics limits the attainable sensitivity of GW detectors. A systematic approach for the design of a feedback controller in the suspension systems of these auxiliary optics is presented in this paper. Experimental validation shows a substantial reduction in the RMS velocity compared to the feedback strategy currently employed in these suspension systems.**

***Index Terms*—Gravitational Waves, Virgo, MultiSAS, scattered light, feedback control.**

I. Introduction

Gravitational Wave (GW) detectors are used to gather knowledge on violent cosmic events like the merger of pairs of black holes. These waves are measured using large-scale interferometers, which detect the undulations in *spacetime* resulting from GWs. The two largest GW detectors are Virgo [1] and LIGO [2], of which the latter measured the first GW in 2015 [3], resulting from the merger of two black holes.

Among the most dominant disturbances in GW detectors is scattered light noise, caused by the residual motion of auxiliary optics in the detector [4]. This residual motion is primarily induced by ground motion, for which suspension systems have been designed to reduce their effect. However, these suspension systems only provide passive attenuation above the eigenfrequency of the isolation stages, whereas scattered light is a function of the RMS motion of the optical components. Low frequency residual motion can therefore at times limit the detector sensitivity, particularly during increased seismic activity resulting from e.g. bad weather.

Reducing the low frequency motion of these optical components can be done through the use of active control of the isolation stages. The subject of this paper is the control design for the suspension used to isolate the auxiliary optics in Virgo, which was found to be the main source of scattered light noise [5]. A control design for this system was presented in [6] and this design has been used in Virgo for the past couple of years. However, residual motion of this suspension system remains problematic during increased seismic conditions [5]. This is partly because the current controller was not explicitly designed to minimize the RMS motion, but also because the filter design lacks structure in terms of coping with the two dominant disturbances, namely ground translation and ground tilt. There is thus a desire for a more structured control design that further reduces the RMS motion of the auxiliary optics.

The objective of this paper is therefore to present a systematic tuning approach for the design of a feedback controller that focusses on minimizing the RMS motion of the auxiliary optics. To this end, the following three contributions are made

C1: Delineation of the control problem in view of the high level system functionality.
C2: Development of a systematic tuning approach for the design of the feedback loops.
C3: Experimental verification of the proposed control design on a prototype suspension system.

The outline of this paper is as follows. Section II will present an overview of the system and delineate the control problem. A systematic tuning approach for the feedback controller will then be presented in Section III. Experimental validation of the new controller design as well as a performance comparison to the currently employed feedback strategy is then presented in Section IV. Conclusions on the findings and future research is presented in Section V.

II. System description

This section relates the high-level functionality of a GW detector to the control problem of the suspension system in minimizing scattered light noise. In Sub-section II-A, a top-down overview of the system is given, from high level system functionality down to the role of the responsible control system in mitigating scattered light noise. Sub-section II-B will then delineate the control problem.

A. Top-down system overview

GWs produce undulations in *spacetime* that stretch all constituents of space in one direction and squeeze it in the orthogonal direction. The detectors measure these undulations by monitoring the difference in length between two orthogonal arms using interferometry. In Virgo, these arm lenghts are $3\,\mathrm{km}$ long and the induced change in length of the arms by a GW is roughly $10 \times 10^{-18}\,\mathrm{m}$. To achieve such extreme levels of precision, a very complex interferometer configuration is

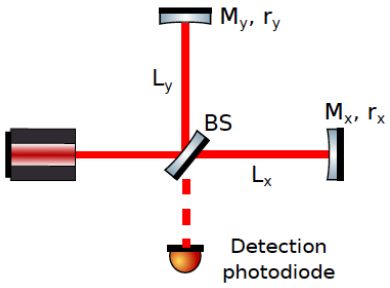

Fig. 1. Simplified configuration of a Michelson interferometer used in Gravitational Wave detectors [7].

used of which the basic underlying principle will be discussed next.

In Fig. 1, a simplified configuration of a GW detector is shown, which in essence is a form of a Michelson interferometer. A laser beam (left) shoots a beam of light through the Beam Splitter (BS) mirror, which splits the beam into two orthogonal directions (upwards and to the left). Both beams are reflected back by the end mirrors M_{x}, M_{y} and interfere at the BS mirror. The interference pattern is a function of the difference between the two arm lenghts L_{x}, L_{y} and this pattern is measured using the detection photodiode. When a GW passes, one arm length increases while the other arm length decreases, hence changing the interference pattern.

In order to distinguish a GW from other disturbances, the mirrors have to be isolated from these disturbances such that the relative change in distance between the mirrors remains sufficiently small. Suspension systems are therefore used to isolate the mirrors from ground vibrations and the system operates in vacuum to mitigate acoustic effects. The distance of the arms L_{x}, L_{y} is furthermore actively controlled. A relative arm length measurement can be obtained through the use of additional photodiodes placed behind the end mirrors, which is then used by actuators on the mirrors to correct the mirror positions. The photodiodes also require isolation from environmental disturbances and therefore have their own suspension system. Both the mirror and photodiode suspension systems use passive harmonic oscillators, which isolate the optics from ground vibrations above the resonance frequency of the harmonic oscillators. However, the relative RMS velocity between a mirror and corresponding photodiode induces scattered light noise [4], which is a non-linear effect. Low frequency relative motion, resulting from seismic activity, therefore introduces high frequency noise inside the detection band of the detector.

The Virgo detector specified a requirement of $0.5\,\mu\mathrm{m/s}$ RMS as the maximum relative velocity between the mirror and corresponding photodiode, for which scattered light remains negligible [5]. Since ground motion is the main source of low frequency excitation, the RMS velocity of the optics heavily depends on environmental conditions. Seismic measurements gathered over several years at the Virgo site showed that the seismic activity stays below $5\,\mu\mathrm{m/s}$ RMS 90% of the time.

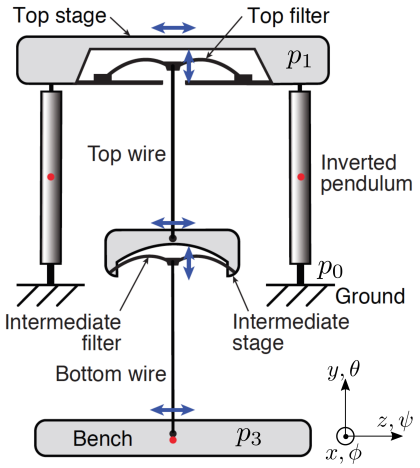

Fig. 2. Schematic overview of MultiSAS, highlighting the passive horizontal and vertical isolation stages that suspend the bench.

Therefore, for scattered light noise to be negligible 90% of the operation time, the RMS velocity of these optics has to be reduced by a factor 10 by the suspension systems, which will be the objective of the developed control design.

The system responsible for isolating the photodiodes in Virgo is called MultiSAS and a schematic overview of the system is depicted in Fig. 2. The bench houses the photodiode and the lateral velocity of the bench (the z direction) is responsible for scattered light noise. The bench is suspended by three horizontal stages of harmonic oscillators (inverted pendulum, top wire and bottom wire) and two vertical stages (top and intermediate filter) to attenuate ground motion. Voice coil actuators as well as two types of sensors are present to control the top stage in the horizontal in-plane directions (x, z, θ), and the vertical direction (y). The first sensor type measures the differential motion between the top stage and ground through which the top stage position is locked in DC, and the second sensor type measures the inertial motion of the top stage which is used to damp the suspension modes.

B. The control problem

The block diagram of the control problem is depicted in Fig. 3. Only the three horizontal in-plane directions will be considered (x, z, θ), because the y direction is assumed to be well-decoupled. The variable to be controlled is $\bar{p}_1 = [p_{1_x}\ p_{1_z}\ p_{1_\theta}]$ and the variable to be minimized is p_{3_z}, who are related through the transfer matrix $\boldsymbol{\mathcal{T}_{13}} \in \mathcal{R}^{1\times 3}$. The top stage motion is subject to ground motion $\bar{p}_0 = [p_{0_x}\ p_{0_z}\ p_{0_\theta}]$ coupling to the top stage through the transfer matrix $\boldsymbol{\mathcal{T}_{01}} \in \mathcal{R}^{3\times 3}$. The top stage motion is measured by a geophone sensor, providing an inertial sensor reading $\hat{\bar{p}}_1$ which is perturbed by *ground tilt* $\bar{d}_{\mathrm{gt}}$, as will be discussed later. The differential sensor furthermore provides a sensor reading of $\bar{p}_1 - \bar{p}_0$. A feedback controller $\boldsymbol{K^{FB}} \in \mathcal{R}^{6\times 3}$ generates a control signal $\bar{u}$ based on the sensor inputs, which is subsequently translated to a top stage motion through the compliance function $\boldsymbol{\mathcal{C}} \in \mathcal{R}^{3\times 3}$. The objective is thus to design $\boldsymbol{K^{FB}}$ that minimizes the RMS velocity of p_{3_z}.

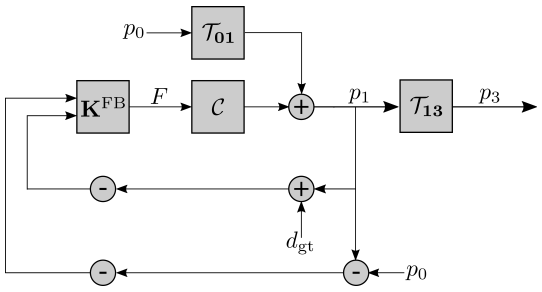

Fig. 3. Block diagram of the control problem.

III. Feedback control design

A systematic tuning approach for the design of the feedback controller $\boldsymbol{K}^{\mathbf{FB}}$ will be presented in this section. First the MIMO control problem is considered in Sub-section III-A, identifying to what extent interaction plays a role and whether this should be taken into account in the control design. Sub-section III-B will then elaborate on the two disturbances present in the system and the implications they have on the control design. The SISO loop design will subsequently be discussed in Sub-section III-C, after which MIMO stability is considered in Sub-section III-D to conclude this section.

A. MIMO identification and decoupling

Identification of the system dynamics has been performed using the inertial sensor since its noise floor is significantly lower compared to the differential sensor. Three sets of co-located actuator and inertial sensor pairs are present on the top stage, which are transformed from their module coordinates to a cartesian coordinate frame, i.e.

$$\boldsymbol{\mathcal{C}} = \boldsymbol{T_y}\boldsymbol{\mathcal{C}}^{\mathbf{m}}\boldsymbol{T_u}. \tag{1}$$

Both $\boldsymbol{T_y}$ and $\boldsymbol{T_u}$ were geometrically determined, which results in the system being decoupled above the highest suspension mode. Open-loop identification of $\boldsymbol{\mathcal{C}}$ has been performed through excitation of each of the cartesian degrees of freedom, resulting in the estimated Frequency Response Function (FRF) depicted in Fig. 4. Although the diagonal terms could be accurately identified in the frequency range of interest, the off-diagonal terms proved to be difficult to identify through the limited dynamic range of the inertial sensors (i.e. the stroke of the proof mass in the geophone), in combination with the the relatively large disturbance of the ground. The coherence was nevertheless sufficiently high to determine the level of interaction between each of the directions. Note furthermore that the diagonal terms for the x and z direction contain the three translational suspension modes, while only the rotational suspension mode of the IP legs is visible for the θ direction.

To quantify the level of coupling, the Relative Gain Array (RGA) [8] is used, which is defined by

$$\boldsymbol{\Lambda(j\omega)} = (\hat{\boldsymbol{\mathcal{C}}}(\boldsymbol{j\omega}) \odot \hat{\boldsymbol{\mathcal{C}}}(\boldsymbol{j\omega})^{-\mathbf{1}})^T, \tag{2}$$

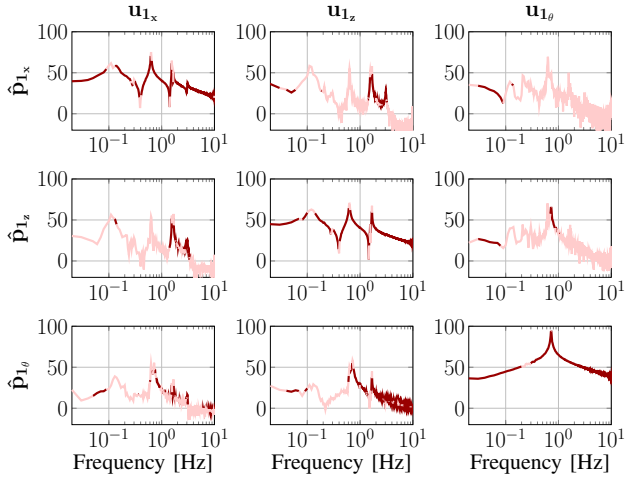

Fig. 4. FRF of the compliance function $\hat{\boldsymbol{\mathcal{C}}}$. (▬) represents frequency bins for which the coherence is > 0.8, while (▬) represents frequency bins for which the coherence is < 0.8. $\hat{\boldsymbol{\mathcal{C}}}$ is measured using the geophones, which output a velocity signal.

where $\odot$ denotes the element-by-element multiplication and $\hat{\boldsymbol{\mathcal{C}}}(\boldsymbol{j\omega})$ is the data-based estimate of $\boldsymbol{\mathcal{C}}$. When $\hat{\boldsymbol{\mathcal{C}}}$ is perfectly decoupled, it holds that

$$|\boldsymbol{\Lambda(j\omega)}| = \boldsymbol{I_3}\ \forall\, \omega \in \mathbb{R}^+, \tag{3}$$

where $\boldsymbol{I_3}$ denotes a 3×3 identity matrix. The RGA for $\hat{\boldsymbol{\mathcal{C}}}$ is depicted in Fig. 5. The θ direction is shown to be well-decoupled from the translational directions (the off-diagonal terms are assumed to be sufficiently decoupled when they are smaller than $-20\,\mathrm{dB}$ across the entire frequency range) and because the ground does not tilt in θ, the contribution of this direction to p_{3_z} is negligible. The x and z direction do exhibit some coupling, particularly around the 1.6 Hz suspension mode and to a lesser extent around the $0.1\,\mathrm{Hz}$ mode. Since the desired control band (i.e. the frequency band with an open-loop gain higher than 1) is between 0.1 and 5 Hz, the coupling cannot necessarily be neglected and MIMO stability thus has to be considered as well. Concluding, the control design for the θ direction will not be discussed in this paper as this direction is sufficiently well decoupled as to not affect p_{3_z}. The control designs for x and z direction can be designed separately, but stability should be considered in a MIMO setting.

B. Ground tilt effect

To obtain an inertial sensor signal, geophones use a proof-mass as an inertial reference frame. The inertial motion of the sensor housing is measured using a differential transducer, measuring the relative motion of the housing with respect to the proof mass. When situated on the ground or a construction parallel to the ground, the sensor is not only subject to the horizontal translational motion of that surface, but also to the tilt of that surface. As a result of the tilting surface, the force of gravity is not perpendicular to the proof-mass motion anymore, hence generating a spurious horizontal sensor reading. The

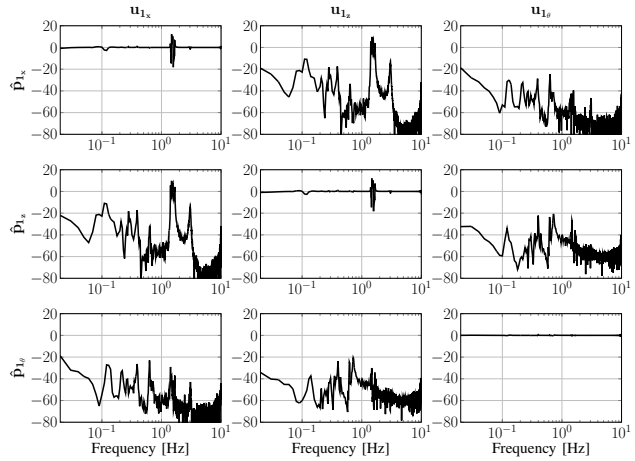

Fig. 5. RGA of the compliance function $\boldsymbol{\mathcal{C}}$.

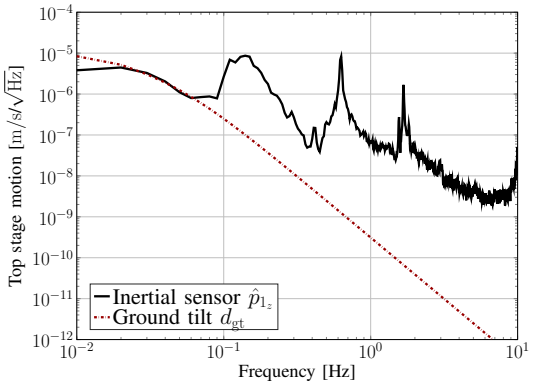

Fig. 6. Inertial measurement of the top stage motion, illustrating the effect of ground tilt on the sensor reading.

reader is referred to [9] for a more elaborate overview, including modelling, of this effect on inertial sensors.

To illustrate the effect of ground tilt on the inertial sensor reading, a measurement of the top stage motion using the geophones is depicted in Fig. 6. The signal $\hat{p}_{1_z}$ represents the measured geophone signal and d_{gt} represents an estimate of the ground tilt effect based on modelling. Above $0.1\,\text{Hz}$, the geophone measures the true horizontal motion of the top stage, while d_{gt} starts to dominate the horizontal sensor signal below this frequency. However, both the amplitude of p_0 and d_{gt} depend on environmental conditions such as wind and oceanic activity, meaning that the frequency above which the geophone provides an accurate reading of the top stage motion varies. Based on literature and measurements on the experimental setup, the conservative estimate was made that $\hat{p}_1$ only provides a sufficiently reliable estimate of p_1 above $0.1\,\text{Hz}$.

C. Loop design

Recall that the objective of the feedback controller is to minimize the RMS velocity of the bench. In Fig. 7, a typical open-loop spectrum of the ground, top stage and bench for

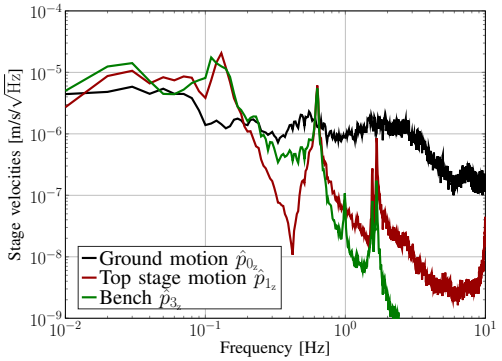

Fig. 7. Typical spectra of the ground, top stage and bench motion in the z direction.

the z direction has been depicted, which shows that the RMS velocity of the bench is dominated by the suspension modes at 0.13 and $0.6\,\text{Hz}$. Because the system is mechanically symmetric in the horizontal plane, the x and z direction transfer functions are almost identical, hence why the same control design will be used for both directions. Furthermore, $\mathcal{T}_{01}$ and $\mathcal{C}$ share the same modes and anti-resonances, while $\mathcal{T}_{13}$ has two resonances at the anti-resonance locations of $\mathcal{C}$ and $\mathcal{T}_{01}$.

The controller design for the x and z direction will be presented next, where the directionality subscript will be tacitly omitted because the derivation holds for both directions. Only the inertial sensor will furthermore be used in the feedback loop as this sensor provides an accurate inertial measurement in the frequency range that dominates the RMS velocity of the bench. Based on Fig. 3 and assuming a SISO system, the closed-loop system can be written as

$$p_3 = \mathcal{T}_{13}\left(S\mathcal{T}_{01}p_0 + T d_{\text{gt}}\right), \tag{4}$$

with

$$S = \left(1 + K^{\text{FB}}\mathcal{C}\right)^{-1}, \quad T = 1 - S. \tag{5}$$

To minimize the effect of ground motion, S should be designed to be small at the frequencies where $\mathcal{T}_{01}p_0$ is high, while minimizing T below $0.1\,\text{Hz}$ to minimize the coupling of ground tilt noise to the output. The bode plot of the open-loop system $K^{\text{FB}}\mathcal{C}$ in the z direction is shown in Fig. 8, reflecting the design considerations to have high gain at the suspension modes and simultaneously having sufficient roll-off below $0.1\,\text{Hz}$ to minimize the amplification of ground tilt noise. The general structure of the controller consists of a lead filter to boost the gain above $0.1\,\text{Hz}$, an inverse notch at $0.13\,\text{Hz}$ and at $0.63\,\text{Hz}$ to provide more damping of the suspension modes, as well as a high and low-pass filter to provide gain roll-off outside the bandwidth of the controller. The Nyquist plot is shown in Fig. 9, which shows no encirclements around the -1 point and hence guaranteeing closed-loop SISO stability. The controller was furthermore designed to provide a modulus margin of $6\,\text{dB}$, which is achieved as the lines do not enter the dashed black circle around the -1 point.

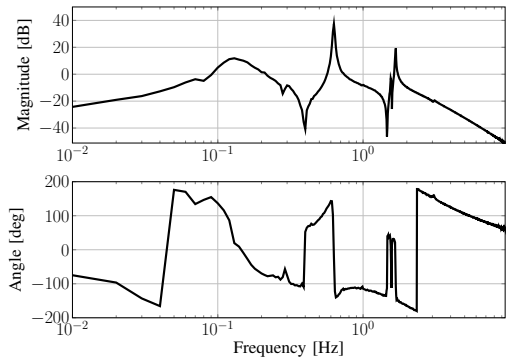

Fig. 8. Bode plot of open-loop $K^{\mathrm{FB}}\mathcal{C}$ for the z direction, illustrating high gain at the suspension modes in combination with gain roll-off at the frequencies where ground tilt noise is dominant.

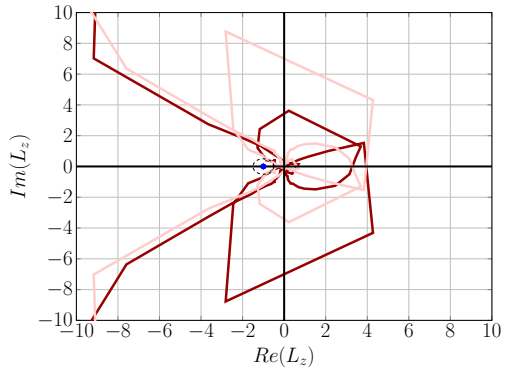

Fig. 9. Nyquist plot of open-loop $K^{\mathrm{FB}}\mathcal{C}$ for the z direction, with (▬) representing positive frequency bins and (▬) representing negative frequency bins. No encirclements of the -1 point can be observed, hence proving closed-loop stability.

D. MIMO stability

To assess the stability of the controllers in a MIMO setting, the characteristic loci are individually evaluated on the Nyquist criterion [10]. This is a generalization of the SISO Nyquist criterion, where the system is closed-loop stable if $\bar{\lambda}(\boldsymbol{L}(\boldsymbol{j\omega})) = [\lambda_1(\boldsymbol{L}(\boldsymbol{j\omega}))\ \lambda_2(\boldsymbol{L}(\boldsymbol{j\omega}))\ \lambda_3(\boldsymbol{L}(\boldsymbol{j\omega}))]^T$ have no encirclements of the -1 point. The θ direction is also considered for completeness and the MIMO Nyquist plot is shown in Fig. 10. Even though the frequency spacing is quite large, the conclusion can still be drawn that no encirclements of the -1 point are made. It can however be observed that some dots are within the $6\,\mathrm{dB}$ circle around the -1 point, while the Nyquist plot of the SISO system stayed outside this circle. The dots that are in the circle are the frequencies around 0.1 and $1.6\,\mathrm{Hz}$, where there is significant interaction between the x and z direction. The dots are nevertheless sufficiently far from the -1 point as to not compromise stability and robustness.

IV. Experimental results

The new controller design has been tested on a MultiSAS test rig, available at the Nikhef facility in Amsterdam. The test rig has six additional geophones placed on the bench to assess the performance of the system and a seismometer is

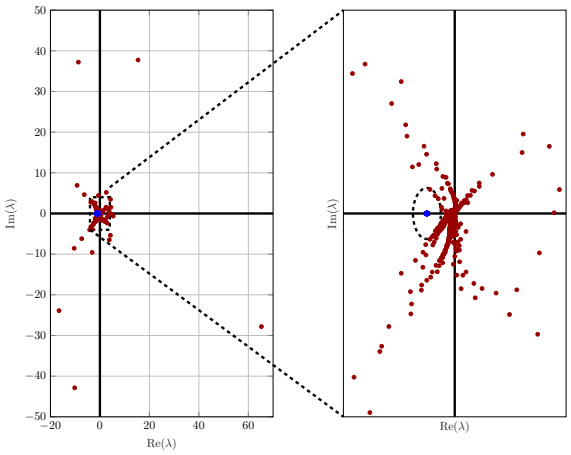

Fig. 10. MIMO Nyquist stability criterion assessed for $\bar{\lambda}(\boldsymbol{L}(\boldsymbol{j\omega}))$. All three eigenvalues in $\bar{\lambda}(\boldsymbol{L}(\boldsymbol{j\omega}))$ are plotted in the same plot as dots. The negative frequency bins are not visualized for clarity of presentation. Visually connecting the dots yields no encirclement of the -1 point, hence proving MIMO closed-loop stability.

available on the ground to measure the disturbance spectrum. The performance will be assessed using a band-limited RMS (bRMS) definition, i.e.

$$p_{3_z}^{\mathrm{bRMS}} = \sqrt{\int_{0.1}^{10} P_{3_z}^2(f)df}, \tag{6}$$

with $P_{3_z}^2(f)$ the Auto Power Spectral Density of p_{3_z}. The band-limited definition is used because the geophones are not reliable below $0.1\,\mathrm{Hz}$.

First, the attenuation properties of the system are assessed by evaluating the motion of the ground, top stage and bench in the z direction, as depicted in Fig. 11. The ground motion has a bRMS of roughly $2.4\,\mu\mathrm{m/s}$, whereas both the top stage and bench bRMS are at roughly $0.6\,\mu\mathrm{m/s}$, thus yielding a factor 4 attenuation of the ground motion with respect to the bench.

The newly proposed feedback strategy is furthermore compared to the original feedback strategy proposed in [6]. The original feedback strategy uses blending filters to create a single sensor signal, composed of the differential sensor at low frequencies and inertial sensor at high frequencies (the reader is referred to [6] for a full overview of the control design). The downside of this strategy is that the differential sensor cannot be used at frequencies where ground motion is high (which is above $0.1\,\mathrm{Hz}$) because this sensor couples the top stage to the ground, whereas the inertial sensor cannot be used below $0.1\,\mathrm{Hz}$ as a result of the ground tilt coupling. The blending frequency (i.e. the frequency where the inertial sensor takes over as the primary sensor) was placed around $0.1\,\mathrm{Hz}$, which resulted in some coupling of the top stage to the ground above $0.1\,\mathrm{Hz}$, while also amplifying ground tilt noise through the inertial sensor. The new strategy therefore uses separate controllers for each sensor (the differential sensor and geophone), which results in no control action between

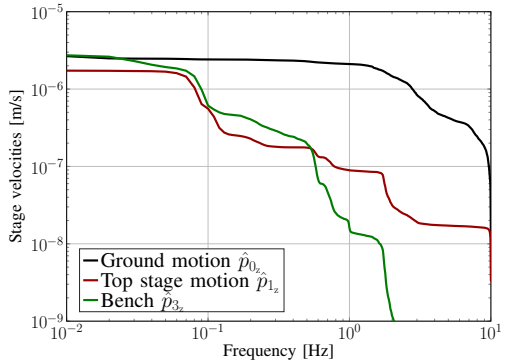

Fig. 11. Cumulative RMS of the new feedback strategy measured at the ground, top stage and bench. The bRMS value is the datapoint on the lines at 0.1 Hz. A factor 4 reduction of the bRMS ground motion with respect to the bench motion can be observed.

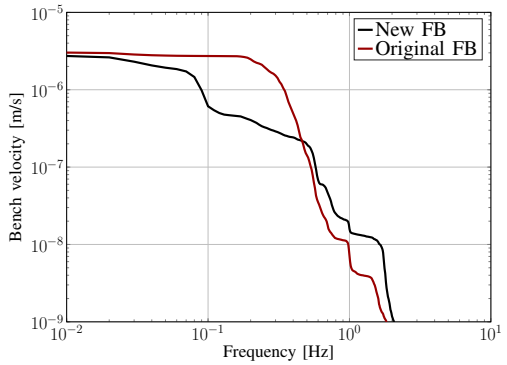

Fig. 12. Cumulative RMS comparison between original and newly proposed feedback strategy. A factor 4 improvement in terms of the bRMS can be observed.

0.01 and 0.1 Hz. Because there is no significant disturbance perturbing the top stage in this frequency band, the bRMS value is expected to be reduced with this new strategy.
Fig. 12 depicts the cumulative RMS of the two controllers. The new feedback controller outperforms the original feedback strategy between 0.1 and 0.5 Hz by roughly a factor 10, at the expense of some performance loss above 0.5 Hz. The bRMS of the new feedback strategy is a factor 4 better, which indeed results mainly from the choice of splitting the sensor signals into two separate feedback loops.
The largest contribution to the bRMS motion of the bench with the new feedback controller is still around 0.1 Hz, which is around the bandwidth of the controller. Further improving the attenuation properties around this frequency in the presence of ground tilt noise therefore becomes difficult, as increasing the gain around 0.1 Hz will inherently lead to more amplification of ground tilt noise below 0.1 Hz.

V. Conclusions

The work presented in this paper entails the design of a feedback controller for MultiSAS, which aims to minimize scattered light noise in Virgo. The objective of this feedback controller is to minimize the RMS horizontal bench motion, which requires attenuation of ground motion below the highest suspension mode. The presented approach illustrates a step-by-step analysis of the control problem including relevant design considerations for the feedback controller.

First, the interaction analysis showed that although the loop designs can be done in a SISO setting, a MIMO stability analysis is necessary due to coupling between the x and z direction around the desired crossover frequencies. The θ direction was shown to be sufficiently decoupled as to disregard it in the control design for the minimization of the bench z motion. Design considerations for the filters have furthermore been discussed with the focus on how to cope with the two dominant disturbances in ground translation and ground tilt, which present conflicting requirements on the control design. Finally, a MIMO stability analysis has been presented, illustrating that the system is also closed-loop MIMO stable.

Experimental results on a prototype system showed a significant reduction in the bRMS motion from ground to bench. A comparison was furthermore also made with the original control strategy, which is currently employed at the MultiSAS systems in Virgo. These experimental results also showed a substantial reduction in the bRMS motion of the bench, which mainly stems from the choice of splitting the two control loops for the differential and inertial sensor.

Further performance improvement is mainly limited by ground tilt motion coupling to the inertial sensors. The LIGO detector already employs an inertial ground tilt sensor in the feedback loop to subtract the ground tilt effect from inertial sensors [11]. This method shows promising results and future research will focus on similair and alternative methods to negate the ground tilt effect.

References

[1] F. Acernese *et al.*, "Advanced Virgo: a second-generation interferometric Gravitational Wave detector," *Classical and Quantum Gravity,* vol. 32, no. 2, p. 024001, 2014.

[2] J. Aasi *et al.*, "Advanced LIGO", *Classical and Quantum Gravity,* vol. 32, no. 7, p. 074001, 2015.

[3] B. P. Abbot *et al.*, "Observation of Gravitational Waves from a Binary Black Hole merger," *Phys. Rev. Lett.,* vol. 116, p. 061102, 2016.

[4] T. Accadia *et al.*, "Noise from scattered light in Virgo's second science run data", *Classical and Quantum Gravity,* vol. 27, no. 19, p. 194011,

[5] A. Bertolini, "Technical noise from SBE: Controls of the end benches suspensions," Tech. Rep. VIR-0883B-19, Virgo Collaboration, 2019.

[6] J. V. Heijningen *et. al.*, "A multistage vibration isolation system for Advanced Virgo suspended optical benches", *Classical and Quantum Gravity,* vol. 36, no. 7, p. 075007,

[7] J. C. Diaz, *Control of the Gravitational Wave Interferometric Detector Advanced Virgo.* PhD thesis, Université Paris-Saclay, 2018.

[8] E. Bristol, "On a new measure of interaction for multivariable process control," *IEEE Transaction on Automatic Control,* vol. 11, no. 1, pp. 133–134, 1996.

[9] B. Lantz, R. Schofield, B. O'reilly, D. E. Clark, and D. DeBra, "Review: Requirements for a ground rotation sensor to improve Advanced LIGO," *Bulletin of the Seismological Society of America,* vol. 99, pp. 980–989, 2009.

[10] S. Skogestad and I. Postlethwaite, *Multivariable Feedback Control.* Wiley, 2 ed., 2005.

[11] K.Venkateswara *et al.,* "Subtracting tilt from a horizontal seismometer using a ground-rotation sensor," *Bulletin of the Seismological Society of America*, vol. 107, 2017.